https://doi.org/10.1016/j.ijheatmasstransfer.2016.06.052

On the role of droplet bouncing in modeling impinging sprays under elevated pressures

Zhenyu Zhang[a], Yicheng Chi[a], Longji Shang[a], Peng Zhang[a*], Zhenfeng Zhao[b]

[a] *Department of Mechanical Engineering, The Hong Kong Polytechnic University, Kowloon, Hong Kong*

[b] *School of Mechanical Engineering, Beijing Institute of Technology, Beijing, PR. China*

Abstract: Impingement of multiple diesel sprays under an elevated pressure of 30atm is investigated numerically and experimentally, with the particular interest in illustrating the importance of taking into account of the ambient pressure effects in modeling binary droplet collisions. Specifically, a practical while simplified droplet collision model was proposed by modifying the widely-used Estrade et al.'s model to account for the previous experimental observation that hydrocarbon droplets tend to bounce back upon collision at elevated ambient pressures. The KIVA-3V program code implemented with the model was used to simulate the impinging sprays from the previous and the present experiments. The results show that the present model can produce qualitatively satisfactory predictions to the shape, the penetration length, and the Sauter mean diameter (SMD) of the impinging sprays because it accounts for the increased propensity of droplet bouncing at elevated pressures, which however was not considered in any previous models. Due to the limited experimental data on binary droplet collision at elevated pressures, the present model can be treated as a practical approximation for predicting droplet collision outcomes in sprays under high-pressure engine conditions.

Keywords: Droplet collision, Bouncing, Impinging sprays, High pressure, KIVA-3V.

* Corresponding author.
E-mail: pengzhang.zhang@polyu.edu.hk
Fax: (852)23654703 , Tel: (852)27666664.

1. Introduction

Dispersion of a liquid into a gaseous environment is a basis for numerous industrial processes, such as various liquid sprays used in metallurgical, chemical, pharmaceutical and food engineering [1]. The elementary role of droplet collision in influencing the spraying processes has been well recognized and extensively studied [2]. A prominent example is the binary collision of fuel droplets under compression-ignition engine conditions. The high number density of fuel droplets and the non-uniform turbulent flow in the combustion chamber imply frequent droplet collisions. The collision outcomes, such as bouncing, coalescence and separation, can substantially affect the spray characteristics and the subsequent vaporization, combustion and emission [3].

As a fundamental phenomenon relevant to many natural and industrial processes, binary droplet collision has been extensively studied for decades. A large number of experimental studies has been reported in the literature [4-13] and summarized in a few excellent reviews [14,15]. The majority of the studies were focused on identifying various collision outcomes and quantifying their dependence on the non-dimensional controlling parameters, such as the collision Weber number, *We*, measuring the relative importance of droplet inertia compared to its surface tension; the impact parameter, *B*, characterizing the deviation of droplet trajectory ($0< B \leqslant 1$) from that of head-on collision ($B=0$); and the size ratio, Δ, defined by the ratio of the diameter of the larger droplet to that of the smaller one. Additional parameters such as the density and viscosity ratios of liquid and gas may be needed when the effects of the other physical properties of the liquid and the ambient gas are taken into account [13].

The earlier studies on the equal-sized water droplets under atmospheric pressure [5, 6] show that the collision results in either coalescence or separation, depending on *We* and *B*. The experimental studies of Jiang et al. [7] and Qian and Law [8] on the equal-sized droplets of n-alkanes identify five distinct collision regimes, namely (I) coalescence after minor deformation, (II) bouncing, (III) coalescence after substantial deformation, (IV) coalescence followed by separation for near head-on

collision (a.k.a. reflective separation), and (V) coalescence followed by separation for off-center collision (a.k.a. stretching separation). The five regimes were subsequently confirmed by Estrade et al. [9] for ethanol.

As a phenomenon of practical relevance, collision between two unequal-sized droplets has not been sufficiently studied compared with that between two unequal-size droplets. The size ratio has been found to have significant influence on the collision outcomes. Ashgriz and Poo [10] experimentally found that water droplet separation becomes more difficult as the size ratio increases. This work was subsequently examined for water [11] and extended for ethanol droplets [9]. The experimental and theoretical study by Tang et al. [12] demonstrates that the suppression of the increased size difference on droplet separation attributes to the increased viscous dissipation and exists not only for water but also for hydrocarbon fuels.

The regime nomogram in the *We*-*B* parameter plane can be significantly affected by the ambient gas pressure, as shown in Figure 1, where n-tetradecane is used as an example. The coalescence regime (I) is observed at atmospheric pressure while it becomes smaller at 2.4 atm and eventually absent with increasing the pressure to 4.4 atm. Similarly, the bouncing regime (II) is observed at atmospheric pressure while it is absent for small *B* and at lower pressures such as 0.7 atm. Furthermore, the critical Weber number separating the bouncing regime (II) and the coalescence regime (III) is substantially increased at elevated pressures. All of these observations indicate that droplet bouncing is promoted by increasing the ambient pressure because the increased inertia of the gas film separating the droplet surfaces suppresses the gas drainage and hence promotes bouncing [13].

Because of its important role in modeling spray characteristics, droplet collision model is an indispensable component in the Lagrangian simulation of the spray processes in compression-ignition engines. The challenges of modeling droplet collision originate from the difficulties in predicting the collision probability [16,17], in parameterizing the complex collision outcomes [18],

and in determining the post-collision characteristics of droplets [19,20]. In spite of the experimental discoveries and theoretical advances made in the past decades, our understanding of the fundamental processes of binary droplet collision is far from being complete.

The widely used KIVA-3V computer program for simulating compression-ignition engine combustion adopts O'Rourke's droplet collision model [21]. Based on Brazier-Smith et al.'s [6] experimental observations on water droplet collisions, O'Rourke's model estimates the critical impact parameter, B_{cr}, as a function of *We* and Δ, and compares it with a randomly selected B to determine whether a collision results in separation ($B > B_{cr}$) or coalescence ($B \leqslant B_{cr}$). Because it is over-simplified in accounting for collision outcomes, O'Rourke's model was improved in many subsequent modeling efforts. For a brief summary, Tennison et al. [22] and Aumann et al. [19] extended O'Rourke's model by taking into account of the reflexive separation. Estrade et al. [9] subsequently proposed a *We*-based model for predicting bouncing. More sophisticated models accounting for bouncing, coalescence, reflexive separation and stretching separation were developed by Kollar et al. [23] and Post and Abraham [20]. Because these models do not consider droplet fragmentation, which often occurs at sufficiently high Weber numbers, predictive models for droplet fragmentation were proposed by Georjon and Reitz [24] and Brenn et al. [25]. In recent years, Munnannur and Reitz [26-28] developed a new predictive model for fragmenting and non-fragmenting binary droplet collisions within engine fuel sprays. More detailed summary can be found in Munnannur and Reitz [26] and Kim et al. [29].

The present study was motivated by modeling the impinging sprays in the opposed-piston compression ignition engine (OPCI) [30] for its potential in achieving high indicate thermal efficiency and good balance performance. Since cylinder head is absent in OPCI, fuel injectors can only be installed on the cylinder liners and sprays from each injector impinge with each other in the combustion chamber, as is shown in Figure 2. The increasingly significant role of droplet collision in OPCI can be understood by recognizing that the collision frequency of droplets is substantially increased due to the impingement of sprays compared with that in the nearly non-interacting sprays

used in the four-stroke compression ignition engines. The characteristic of impinging sprays in OPCI was numerically studied by using Star-CD with O'Rourke's model [31-34]. Lee et al. [35] proposed a model to account for the increased collision frequency in OPCI, which was subsequently modified by Ko and Ryou [36] to include the satellite droplet formation. Kim et al. [29] developed a predictive model including most of the collision outcomes to simulate the impinging sprays at 10 atm, which were experimentally studied by Chiba [37] and Maruyama [38].

In spite of these advances in modeling droplet collision in either non-interacting or impinging sprays, the influence of the ambient pressure on droplet collision outcomes and hence the spray characteristics in compression-ignition engines have been barely studied. It can be expected that the propensity of droplet bouncing can be substantially enhanced as the gas pressure in the combustion chamber increases to 10-30 atm at the end of the compression stroke. In addition, the critical Weber numbers for droplet coalescence and separation may be so high at elevated pressures that these collision outcomes are unlikely to occur. However, it is surprising to find that only a very few studies on binary droplet collision have been carried out under the non-atmospheric pressure conditions, posing great difficulty on modeling. Willis and Orme [39] experimentally studied the collision of oil droplets in vacuum to investigate the role of viscosity. Qian and Law's experiments under the pressures of 0.6-13.6 atm show that increasing pressure promotes bouncing while decreasing pressure promotes coalescence. Zhang and Law's [13] theoretical analysis demonstrates that, as increasing the ambient gas pressure, the gas between the two droplets becomes denser and harder to be drained out. As a result, substantially increased pressure buildup and droplet deformation suppress the droplet coalescence and therefore promote droplet bouncing. It is noted that Dupuy et al. [40] applied the Lattice Boltzmann method combined with a free energy approach to simulate the head-on collision of two-dimensional droplets up to 150 bar. However, their results have not been substantiated by any experiments.

Based on the above considerations, we conducted a numerical and experimental investigation of impinging sprays at elevated pressures up to 30 atm, with emphasis on illustrating the necessity of

considering the gas pressure effects in modeling droplet collision, particularly droplet bouncing. We shall describe the adopted numerical methodology based on the KIVA-3V program and develop a practical albeit simplified model for droplet collision at elevated pressures based on the experimental results of Qian and Law [8], in Section 2. The experimental specifications shall be presented in Section 3, followed by the validation of the simulation against the available experimental data in the literature, in Section 4. We shall then present, in Section 5, the experimental results and numerical simulation of impinging sprays at a pressure of 30 atm.

2. Modeling Droplet Collision at Elevated Pressures in KIVA-3V

The widely used KIVA-3V computer program was adopted in the present study for the Reynolds Average Navier-Stokes (RANS) calculation of non-reacting turbulent flows with sprays. In the spraying process, liquid fuel is injected into the chamber in the form of liquid droplets of the nozzle size. The TAB model [41] and Spalding model [42] were used to account for the subsequent droplet breakup and evaporation, respectively. The standard k-ε model [21] was used for modeling turbulence. It is noted that the present study does not aim to employ and compare the more sophisticated models for droplet breakup and evaporation and for turbulent flows, which have been extensively studied in the literature [2]. Consequently, the standard numerical schemes and models implemented in KIVA-3V were used to facilitate the comparison of droplet collision models with and without considering the ambient pressure effects, to be elucidated in the following text.

The collision Weber number, the impact parameter and the droplet size ratio are usually used for parameterizing the droplet collision outcomes. The Weber number is defined as $We=\rho U^2 r_1/\sigma$, where ρ is the droplet density, U the relative velocity, r_1 the radius of the smaller droplet and σ the surface tension coefficient. The size ratio is defined as $\Delta=r_2 / r_1$, where r_2 is the radius of the larger droplet. The impact parameter is defined as $B=X / (r_1+r_2)$, where X is the projection of the distance between the droplet centers in the direction normal to that of the relative velocity. To account for the

experimental observation of Qian and Law [8], namely, increasing the ambient pressure promotes droplet bouncing, the widely used bouncing criterion of Estrade et al. [9]

$$We < \frac{\Delta(1+\Delta^2)(4\Theta'-12)}{\chi_1\{\cos[\sin^{-1}(B)]\}^2} \tag{1}$$

the RHS of which is equal to 2.8 for Δ=1 and B=0, is modified by adding a pressure-dependent multiplication factor g(p) as

$$We < We_{cr}(p, \Delta, B) = g(p)\cdot We_{cr}(1,1,0)\frac{\Delta(1+\Delta^2)(4\Theta'-12)}{2.8\chi_1\{\cos[\sin^{-1}(B)]\}^2} \tag{2}$$

In the equation, $We_{cr}(1,1,0)$ is the bouncing-coalescence transition Weber number for head-on collision at p=1 (in atm), Δ=1 and B=0; a normalization factor of 2.8 is therefore needed in the denominator of the Estrade et al.'s formula; the shape factor Θ'=3.351 and χ_1 is determined by χ_1=1-0.25(1+τ)(2-τ)^2 if $(r_1+r_2)(1-B)>r_1$, otherwise, χ_1=0.25(3-τ)τ^2, where τ=(1-B)(1+Δ). The pressure-dependent factor g(p), defined so that g(1)=1, is assumed to be "liquid-independent" because the liquid-specific collision outcomes have been reflected in $We_{cr}(1,1,0)$ and the Estrade et al.'s formula. Consequently, the pressure factor can be obtained by fitting the experimental data of Qian and Law's [8] for the bouncing-coalescence transition Weber numbers for n-tetradecane and water, at various pressures, and with fixed Δ=1 and B=0.

In order to minimize the uncertainty of the pressure factor, g(p) was fitted in three power-law formula such as g(p)=ap^{β}+b with β=0.5, 1.0 (linear) and 2.0. As shown in Figure 3, the fitting formula obtained are g(p)=1.03$p^{0.5}$-0.03 with the coefficient of determination R^2=0.584, g(p)=0.25p+0.75 with R^2=0.529, and g(p)=0.02p^2+0.98 with R^2=0.342. Because of the paucity of the available data and the limited range of pressures from 1.0 atm to 13.6 atm, the factors can be considered as practical, nevertheless, physically justifiable approximations for accounting for the pressure-dependence.

In the present study, we extrapolated the factor up to 30 atm, at which additional experimental validation is needed while not available up to now. Two shadow regions are indicated in Figure 3, representing the "experimentally unavailable" one on the right, in which no experimental data are available in the literature, and the "theoretically inaccessible" one on the bottom, in which additional physics is needed to explain the experimental data with g(p)<1. Qian and Law [8] observed the suppression of droplet bouncing (i.e. g(p)<1) in the presence of fuel vapor or similar fuel gases, and attributed it to the modified surface tension of droplets. Since the present study considers the impinging sprays in unheated environments, droplet vaporization is assumed to be negligible during the impingement process. Consequently, the present model does not consider the effects of fuel vapor on the collision outcomes, which nevertheless merit future studies. Thus, the experimental data in the "theoretically inaccessible" area were not included in the present fittings.

It has been recognized that droplet collisions are inelastic and the viscous dissipation in the deformed droplets upon collision can be as large as 50% of the initial kinetic energy of droplets for sufficiently large Weber numbers [8]. Tang et al.'s [12] experimental study on unequal-size droplet collision also confirmed that the viscous dissipation during the initial collision stage slightly varies with the size ratio [12]. Consequently, we accounted for the influence of viscous dissipation on the bouncing droplets by expressing the post-collision velocities by

$$u_{n,i}=\frac{u_i r_i^3+u_j r_j^3+r_j^3(u_i-u_j)\sqrt{1-f_{\mathrm{E}}}}{r_i^3+r_j^3} \quad (i,j=1,2) \tag{3}$$

where u is the droplet velocity, the subscript n denotes the droplets after coalescence. The derivation of the equation has been described in detail by O'Rourke [43] by accounting for the conservation of both momentum and energy during the droplet collision. A fraction of energy dissipation, which is denoted by f_{E} in O'Rourke's notation, is taken into account in the energy conservation. In lieu of O'Rourke's assumption on correlating f_{E} with other collision parameters, we used f_{E}=0.5 as a maximum value observed in the previous experiments [7].

As discussed in the Introduction, droplet separation can be substantially suppressed with increasing the ambient pressure. Consequently, we consider only coalescence and bouncing in the present model by assuming the probability of droplet separation is negligibly small as the pressure increases to 10-30 atm. The present study does not intent to establish a comprehensive and predictive model accounting for all the possible collision outcomes under wide ranges of conditions. Instead, its primary purpose is to illustrate the necessity of modifying the exiting droplet collision models to take into account the effects of ambient pressure and therefore advocate future experimental studies on binary droplet collision at elevated pressures.

3 Experimental Specifications

In the following section, the present droplet collision model shall be validated against Maruyama's [38] experiments on impinging sprays of light oil at 10atm. In order to extend the validation to a higher ambient pressure and under a more practical situation, we designed and conducted an experiment for multiple impinging sprays of diesel, as shown in Figure 4. Two opposed 10mm×10mm windows (1) of optical glass JGS-1 are placed on the chamber (2). A Bosch CP1H3 common rail system (3) of about 160.0 MPa is employed as the fuel supply system. The oil pump (5) is driven by an EBS677 electrical motor (6) with the maximum theoretical power of 30kW and an actual operating power of about 8kW was employed to pump diesel from the oil tank (7) to the common rail through filters (8). Two three-nozzles (0.2mm in diameter), Bosch CRI2.2 injectors (4) are controlled by the control system (16) and the injection period is1.5ms. In order to stabilize the chamber pressure at 30 atm, the high-pressure nitrogen stored in a cylinder (9) enters into a regulator tank (11) through a Gentec U53SL reducing valve (10), and then goes through the valve (12) to enter into the chamber (2), which is monitored by a pressure meter (15). A stroboscope (13) is used as the light source for the shadowgraph images taken by a Fastcam SA4 camera (14) with 10000 fps. The injection and visualization systems are synchronized and controlled by the control system (16). In

Figure 4, the red, green and blue lines represent the oil pipes, the signal transmission lines and the gas pipes, respectively.

4. Experimental Validation of Numerical Simulation

To validate the present KIVA-3V simulation and the proposed droplet collision model at elevated pressures, we simulated Maruyama et al.'s experiments on the free and impinging sprays in a constant-volume chamber filled with nitrogen of 10 atm. In the impinging spray experiments, two spray cones are injected from two nozzles of 0.25 mm in diameter for 2.0 ms. The axes of the spray cones are perpendicular to each other to form an impingement point, as shown in Figure 5. Maruyama et al. [38] defined the spray penetration length as $S_z + S_t$, where S_z is the distance from each nozzle to the impingement point and S_z the distance from the impingement point to the spray tip. The present simulation employs a cubic computational domain of 120mm in each dimension and a uniform Cartesian mesh with 216,000 grid cells of 2mm in size. The evolution of the sprays, each of which initially consist of 5000 droplet parcels, were simulated for totally 5 ms with the computational time step being 2×10^{-3} ms. Boundary effects can be neglected in the present problem because the domain size is much larger than the size of the sprays and the penetration length. Consequently, the domain boundaries can be simply set as isothermal walls of 298 K and with the nonslip conditions for velocity.

It has been recognized that the collision probability estimated in KIVA-3V is sensitive to the grid size as such a larger cell size often results in a smaller probability. Kim et al. [29] studied the effect of the grid size in predicting the droplet collision outcomes and suggested a suitable grid size of $2\times2\times2$ mm^3 for simulating Chiba's [37] and Maruyama et al.'s [38] experiments on impinging sprays. Considering that the spray penetration length is one of the key parameters to be used shortly to compare the present simulation with the previous experiments, we simulated the free spray in Maruyama's experiment and examined the grid-dependence of its penetration length on the mesh

resolution. Figure 6 shows the evolution of the spray penetration length with time for six different meshes from the coarsest 5×5×5 mm^3 to the finest 1×1×1 mm^3. It is seen that the calculated results shows a significant dependence on the cell sizes coarser than 2×2×2 mm^3, beyond which the results seem to "converge" to certain limits and the grid-dependence is substantially reduced. This result confirms the previous observation of Kim et al. [29] and hence the cell size of 2×2×2 mm^3 was used in all the simulations to be discussed shortly, as a compromised choice of accuracy and computation efficiency.

Because of the slight difference of three different power-law fittings at 10atm, we shall use the linear fitting as a representative one in the following discussion. We considered the free spray and the impinging sprays with S_z=14 mm, 33 mm and 50 mm in Maruyama et al.'s experiment. As an illustration of the validation, Figure 7 shows the calculated shadowgraph images and droplet trajectories at three different times for the case of S_z=50 mm, which was also simulated by Kim et al. [29] using KIVA-3V with their droplet collision model. Specifically, the experimental shadowgraphs at t=0.92 ms, 1.92 ms and 2.92 ms are shown in Figure 7(a) and Kim et al.'s results in Figure 7 (b). The present results with different models are shown in Figure 7(c)-(f), where the original O'Rourke's model in Figure 7(c); Estrade et al.'s model in Figure 7(d); the present model with f_E=1 (elastic collision, β =1.0) in Figure 7(e); and the present model with f_E=0.5 (inelastic collision, β =1.0) in Figure 7(f).

It is seen that there is no significant difference among the experiment and simulations at 0.92ms when the spray impingement just occurs. The slightly asymmetric experimental images, which may be due to the possibly imprecise timing control of spray injection in Maruyama et al.'s experiment, should not affect the present comparison. After the spray impingement, O'Rourke's model predicts a greater extent of spray spreading and larger droplet sizes than the other models, as show in Figure 7 (c) at 1.92 ms, and subsequently the impingement of the sprays on the bottom wall at 2.92 ms. This is because the droplets in O'Rourke's model tend to coalesce to form bigger ones, which possess larger inertia and hence enhance the spray penetration. It is also seen that O'Rourke's and Kim et al.'s

models not only overestimate the spray spreading but also generate secondary spray tips at 2.92 ms that are not observed in the experiment. The predictions based on the bouncing-coalescence criteria, adopted by Estrade et al.'s and the present models, are in a good agreement with the experiment in terms of the spray spreading and penetration. This implies that droplet bouncing may account for a large number of collision outcomes at elevated pressures. It is also noted that Kim et al.'s simulation shows a significant discrepancy with the experiment and the other model results. Because all the possible collision outcomes including bouncing, coalescence, separation and fragmentation are considered in Kim et al.'s model, it is difficult to determine the specific roles of these outcomes in resulting in such a large discrepancy. A possible reason may be due to their model for predicting the droplet velocities and directions after collision.

It is recognized that the spray impingement with S_z=50 mm is the only case, for what the experimental and numerical images are available in the literature. To further quantify the comparison between the models considered in the study, Figure 8 shows the time-evolving spray penetration lengths of the free spray and the three impinging sprays. Being consistent with the experimental measurement, the calculated penetration lengths were determined from the numerical shadowgraphs. For the free spray shown in Figure 8(a), it is seen that the calculated penetration lengths based on the four models agree well with the experimental data in the early spraying stage (t=0-0.5 ms), during which the spray is mainly affected by the deceleration and breakup of droplets. After t=0.5 ms, the predictions of O'Rourke's model slightly deviate not only from those of the other models but also from the experimental data. However, Estrade et al.'s and the present models produce similar predictions agreeing with the experimental data in the late spraying stage. These observations can be understood by recognizing that the free spray is injected to an initially quiescent environment, in which the turbulent flow induced by the spray-gas interaction in the pressure chamber is not sufficiently strong. Therefore, the droplet collisions with large impact Weber numbers are unlikely to occur in the free spray. As the result, O'Rourke's model results in an overestimated spray penetration length because droplet collisions are predicted to coalesce to form bigger droplets, which have larger

inertia and hence facilitate the spray penetration. Estrade et al. and the present models produce improved predictions by capturing the tendency of droplet bouncing at elevated pressures. It is also noted that, due to the relatively small Weber numbers of the collisions prevalent in the free spray, neither the pressure-corrected transition Weber numbers nor the corrected post-collision velocities used in the present model make significant difference compared with Estrade et al.'s model.

Figure 8(b)-(d) show the spray penetration lengths for the cases of S_z=14 mm, S_z=33 mm and S_z=50 mm , respectively. Several observations can be made from the comparison among the simulations and experiment as follows. First, all the model predictions agree well with the experimental data in the early stage, during which the sprays behave like free ones and are mainly affected by the deceleration and breakup of droplets. Second, regardless of some discrepancies to be discussed, Estrade et al.'s and the present model predictions agree well with the experimental data over the entire impingement process in all the cases. This again can be attributed to that droplet bouncing dominates the collision outcomes at elevated pressures. Third, moderate discrepancies can be found between Estrade et al.'s and the present models in short periods of time after the spray impingement. Specifically, during t=0.2-0.7 ms in the case of S_z=14 mm shown in Figure 8(b), Estrade et al.'s model predicts a larger penetration length than does the present model (elastic collision, β =1.0), which in turns results in a higher prediction than the present model (inelastic collision, β =1.0). This can be understood by that the impingement of sprays result in an increased number of colliding droplets, which tend to coalesce in Estrade et al's model while to bounce back in the present model, because the latter model has a larger transition Weber number separating the bouncing and coalescence regimes due to the increased ambient pressure. Fourth, the smaller prediction of the present model (inelastic collision, β =1.0), which can be found in all the cases, attributes to the reduced kinetic energies of droplets for spray penetration due to the viscous loss upon collision. Finally, the discrepancies between the prediction of the Estrade et al.'s and the present models decrease with increasing S_z , as seen in Figure 8(c), and become negligible in the case of S_z=50 mm shown in Figure 8(d). This is because the sprays travel a longer distance (i.e. S_z) before

the impingement so that droplets will collide with reduced Weber numbers as the result of their deceleration and breakup. Similar to the case of free spray, the difference between these model predictions are minimized at small Weber numbers.

To supplement the above comparison, Figure 9 compares the predicted Sauter mean diameters (SMD) with the experimental data measured at 2.0 mm above the spray tip at t = 2.0 ms. The experimental data show a trend that SMD moderately decreases with increasing S_z, which is well predicted by Estrade et al.' and the present models. In addition, the present model predictions are within the experimental uncertainties while Estrade et al.'s model slightly overestimates SMD and O'Rourke's model predicts an opposed trend. These results are consistent with the above discussion that both Estrade et al.'s and the present models take into account of the significant role of droplet bouncing while the present models may be quantitatively more accurate by considering the influence of the ambient gas pressure on the transition Weber numbers and that of inelastic collision on the post-collision velocity.

It is recognized that all the validation cases from Maruyama et al.'s experiments were conducted at 10atm, which may be not sufficiently high to manifest the influence of droplet bouncing on the characteristics of impinging sprays under actual engine conditions. This consideration motivated us to extend the above simulations to higher ambient pressures. Figure 10 shows the influences of three different power-law fittings on the time-evolving spray penetration lengths of the free spray and the three impinging sprays at both 20 atm and 30 atm. Besides the characteristics similar to the case at 10atm, all the cases considered here are not sensitive to the particular functional form of the fitting formulas, specifically to the value of β. For free spray shown in Figure 10(a), the spray characteristics is mainly influenced by droplet deceleration and breakup, and slightly by droplet collision. For the impinging sprays shown in Figure 10(b)-(d), the sprays behave like free sprays before the spray impingement occurs. Upon the spray impingement, the significantly decelerated droplets collide with each other at the Weber numbers that are too small compared with $We_{cr}(p)$ at

the elevate pressures to result in droplet coalescence. As a result, the different extrapolation values by the fitting formulas at the elevated pressures make insignificant difference in the simulations.

5. Multiple Impinging Sprays

Multiple impinging sprays were studied by using the present experimental apparatus to further validate the present droplet collision model up to 30 atm. Figure 11 (a) and (b) show the front and top views of the schematic of the multiple impinging sprays, respectively. Each injector consists of three independent nozzles, which are indicated as Nos. 1–3 for the left injector and Nos. 4–6 for the right one. From the front view (i.e. on the X-Z plane), the three nozzles of the left injector are installed asymmetrically so that the angle between No.1 and No. 2 nozzles is 40°, that between No. 2 and No. 3 nozzles is 35°, and No. 2 nozzle deviates from the X-axis by 5°. No.4–6 nozzles and the No. 1–3 nozzles are antisymmetric with respective to the X=0 plane (i.e. the Y-Z plane). From the top view (i.e. on the X-Y plane), the three nozzles of the left injector are installed symmetrically so that No. 2 nozzle aligns with the X-axis and has an angle of 3° with No. 1 and No. 3, respectively. No.4–6 nozzles and the No. 1–3 nozzles are symmetric with respective to the X=0 plane (i.e. the Y-Z plane). It is believed that the multiple, asymmetric impinging sprays can enhance the turbulent flow in the pressure chamber. Figure 11(c) shows the three-dimensional view of the spray shapes depicted by the Lagrangian droplets.

In the experiment, the spray injection begins at t=0.0 ms and ends at t=1.5 ms while the subsequent spray evolution was still recorded by the high-speed camera of 10,000 fps. Figure 12 shows the experimental front-view shadowgraphs at the selected time instants with the time interval of 0.3 ms. The corresponding numerical shadowgraphs overlapped by droplet parcels are shown for the comparison between O'Rourke's model and the present model (inelastic collision, β =1.0). To evaluate the possible influence of the initial SMR on the subsequent spray characteristics, we used 0.1 mm (the nozzle radius), 0.18 mm and 0.35 mm in the simulations. The results after t=3.0 ms are

not shown in the figure because the boundary effect on the simulation results may become significant as the droplets are close to the wall. A complete set of experimental and simulation results during the entire process of 3.0 ms can be found in Figure S 1-6 in the Supporting Material.

It is seen that there is no significant difference between the experimental and simulation results for the spray shapes and penetration lengths, from the injection time to t=1.1 ms, at which the spray impingement is about to occur. Both O'Rourke's and the present models predict satisfactorily the time instant of the spray impingement, indicating that droplets in the early stage are dominated by their deceleration and aerodynamic breakup so that different droplet collision models do not make significant difference, as discussed in the preceding section. However, larger droplets can be observed at t=1.1 ms in the prediction of O'Rourke's model compared with that of the preset model. This is because droplet collisions become frequent upon the impingement so that the O'Rourke's model predicts more droplet coalescence and hence droplets with larger sizes.

The distinct difference in the size and number of droplets between these two model predictions can be clearly seen in the numerical shadowgraphs after the spray impingement starts. At t=2.0 ms, O'Rourke's model predicts a wider spatial distribution of droplets than does the present model while the latter can reproduce the spray shape shown in the experimental image. The subsequent experimental images show that the shadow region is concentrated around the center of the images, implying that fuel droplets tend to gather around the center of the chamber. The present model captures this spray characteristic because it predicts more events of droplet bouncing at the high-pressure environment. As discussed in the preceding section, the bouncing droplets lose a substantial amount of their kinetic energies due to the viscous dissipation upon collision and therefore cannot move further with reduced post-collision velocities. As a result, they tend to stay around the camber center where most droplet collisions occur in the present setup of spray impingement. Furthermore, O'Rouke's model predicts more events of droplet coalescence and the coalesced, larger droplets have larger inertia to move in the chamber and consequently produce a longer penetration length. Such an

over-predicted penetration length by O'Rouke's model results in the wall impingement of droplets, which is however not observed either in the present model prediction or in the experimental image.

It is recognized that the quantitative comparison between the present prediction and the experimental observation is difficult due to the following reasons. First, the Nos. 1 and 4 sprays in the experimental images, such as those at t=0.5 ms, 0.8 ms and 1.1 ms, show slightly larger penetration lengths than those in the simulation. This may be due to the slightly larger nozzle diameters of Nos. 1 and 4 and hence more liquid injection compared with the other nozzles. Second, the long-time behavior of the sprays in the present simulation can be strongly affected by the other factors, such as turbulent flow and droplet vaporization. Third, the penetration length after the spray impingement cannot be precisely defined in either experimental measurement or numerical calculation, rendering a comparison similar to that in Figure 8 is impossible. Finally, the impingement of multiple sprays around the center of the chamber results in a region with high number density of droplets. Measuring the droplet size distribution in the dense spray region poses an immense challenge for the existing optical diagnostics, which will not considered in the present study but certainly merits future investigation.

To facilitate the quantitative comparison between the experiment and numerical simulation results, we developed a grayscale level analysis of shadowgraph images. We converted the experimental shadowgraph images into gray-scale ones as shown in the second row of Figures 12(a)-(b), where the dark areas representing either the droplets or the opaque gaseous species have the grayscale levels below a threshold value such as G_{low}=100. Consequently, we defined a time-dependent ratio $r_d=N_d(t|G<G_{low})/N$, where N is the total number of pixels in the image, and $N_d(t|G<G_{low})$ the total numbers of the pixels that have the grayscale levels G lower, G_{low}. By definition, r_d can be considered as an indicator of the degree of spray spreading. Figure 13 shows r_d of experimental and numerical shadowgraph images at 30 atm with different initial (Sauter mean radius) SMR and for various G_{low}. It is seen that, although the values of r_d slightly vary with initial SMR and G_{low}, the good agreement between the experiment and simulations during 0.0ms-1.5 ms

substantiates the proposed gray level analysis as an effective tool to quantify the spray spreading characteristics. The moderately varying discrepancies between the experiment and simulations after 1.5 ms may be due to the increasing sensitivity of the analysis to G_{low} when the droplets are so dispersed in the chamber that the contrast ratios of the gray level images become smaller.

By using the gray level analysis, we numerically investigated the multiple impinging sprays at 10 atm and 20 atm, as shown in Figure 14. Different fittings formula are compared again because their influence on the simulation may emerge at smaller pressures as the result of reduced droplet deceleration and thereby augmented collision Weber numbers. It is noted that r_d after t=1.8 ms is not shown in Figure 14 because the droplets are so close to the chamber wall that the boundary effects cannot be neglected, as shown in Figure S7 in the Supporting Material. It is seen that r_d is not sensitive to the particular functional form of the fitting formulas, specifically to the values of β. This observation can be explained again by that the substantial deceleration of drops, which move about 1.0ms before collisions, have too small Weber numbers to differentiate fitting formula.

6. Concluding Remarks

A numerical and experimental investigation of the impingement of multiple sprays at 30 atm was conducted in the present study. The primary motivation of the study is to illustrate the necessity of considering the ambient gas pressure effects in modelling the binary droplet collision at elevated pressures, which in turn substantially influences the Lagrangian approach of spray simulation, such as that adopted by KIVA-3V. In the present study, a practical droplet collision model was established by multiplying a pressure-dependent correction factor to the widely-used Estrade et al.'s model, which employs a critical Weber number criterion to predict the droplet collision outcomes in terms of bouncing and coalescence. By recognizing the important experimental observations of Qian and Law [8] that increasing the ambient pressure significantly promotes droplet bouncing and accordingly increases the critical Weber numbers separating the bouncing and coalescence regimes in the *We-B*

parameter space, we proposed the approximate correction factor by fitting the available experimental data as three power-law functions of pressures in the range of 1.0-13.6 atm. The present simulations based on the KIVA-3V program with the modified droplet collision model show good agreement with the previous and the present experimental results on various characteristics of free and impinging sprays at elevated pressures, such as the shape, the penetration length and Sauter mean diameter (SMD). The qualitatively satisfactory predictions of the present model signify the physical phenomenon that colliding droplets at high gas pressures tend to bounce back and however is not accounted for in previous models. It is recognized that the present pressure-dependent model is merely a practical approximation based on a paucity of experimental data in the literature. Furthermore, the particular functional forms of the fitting formulas are found to slightly affects the prediction in the present study. Future experimental and theoretical studies on modeling binary droplet collision at elevated pressures are advocated for its applications in simulating sprays under compression-ignition engine conditions.

Acknowledgement

The work was supported by the Hong Kong Research Grants Council/General Research Fund (operating under contract number PolyU 152217/14E) and in part by Central Research Grants of the Hong Kong Polytechnic University (operating under Contract Nos. G-UA2M and G-UBGA). The simulations were conducted using the resources of the High Performance Cluster Computing Centre, Hong Kong Baptist University.

Reference

[1] N. Ashgriz, Handbook of atomization and sprays: theory and applications, Springer Science & Business Media, 2011.

[2] W.A. Sirignano, Fluid dynamics and transport of droplets and sprays, Cambridge University Press, 1999.

[3] J.B. Heywood, Internal combustion engine fundamentals, Mcgraw-hill New York, 1988.

[4] K.-L. Pan, P.-C. Chou, Y.-J. Tseng, Binary droplet collision at high Weber number, Physical Review E, 80(3) (2009) 036301.

[5] J. Adam, N. Lindblad, C. Hendricks, The collision, coalescence, and disruption of water droplets, Journal of Applied Physics, 39(11) (1968) 5173-5180.

[6] P. Brazier-Smith, S. Jennings, J. Latham, The interaction of falling water drops: coalescence, in: Proceedings of the Royal Society of London A: Mathematical, Physical and Engineering Sciences, The Royal Society, 1972, pp. 393-408.

[7] Y. Jiang, A. Umemura, C. Law, An experimental investigation on the collision behaviour of hydrocarbon droplets, Journal of Fluid Mechanics, 234 (1992) 171-190.

[8] J. Qian, C. Law, Regimes of coalescence and separation in droplet collision, Journal of Fluid Mechanics, 331 (1997) 59-80.

[9] J.-P. Estrade, H. Carentz, G. Lavergne, Y. Biscos, Experimental investigation of dynamic binary collision of ethanol droplets-a model for droplet coalescence and bouncing, International Journal of Heat and Fluid Flow, 20(5) (1999) 486-491.

[10] N. Ashgriz, J. Poo, Coalescence and separation in binary collisions of liquid drops, Journal of Fluid Mechanics, 221 (1990) 183-204.

[11] C. Rabe, J. Malet, F. Feuillebois, Experimental investigation of water droplet binary collisions and description of outcomes with a symmetric Weber number, Physics of Fluids, 22(4) (2010) 047101.

[12] C. Tang, P. Zhang, C.K. Law, Bouncing, coalescence, and separation in head-on collision of unequal-size droplets, Physics of Fluids, 24(2) (2012) 022101.

[13] P. Zhang, C.K. Law, An analysis of head-on droplet collision with large deformation in gaseous medium, Physics of Fluids, 23(4) (2011) 042102.

[14] G. Brenn, Droplet collision, in: Handbook of Atomization and Sprays, Springer, 2011, pp. 157-181.

[15] M. Orme, Experiments on droplet collisions, bounce, coalescence and disruption, Progress in Energy and Combustion Science, 23(1) (1997) 65-79.

[16] O.O. Taskiran, M. Ergeneman, Trajectory based droplet collision model for spray modeling, Fuel, 115 (2014) 896-900.

[17] F. Perini, R.D. Reitz, Improved atomization, collision and sub-grid scale momentum coupling models for transient vaporizing engine sprays, International Journal of Multiphase Flow, 79 (2016) 107-123.

[18] P.G. Aleiferis, M. Ashrafi-Nik, N. Ladommatos, G. Dober, K. Karimi, A Study of Droplet Collision Modelling for Spray Formation and Mixing with a Two-Row Group-Hole Injection Nozzle for Diesel Engines, Atomization and Sprays, 24(12) (2014).

[19] R. Aumann, M. McCracken, J. Abraham, An Evaluation of a Composite Model for Predicting Drop-Drop Collision Outcomes in Multidimensional Spray Computations, in, SAE International, 2002.

[20] S.L. Post, J. Abraham, Modeling the outcome of drop–drop collisions in Diesel sprays, International Journal of Multiphase Flow, 28(6) (2002) 997-1019.

[21] A. Amsden, P. O'Rourke, T. Butler, K. II, A computer program for chemically reactive flows with sprays, Los Alamos National Laboratory Rep, LA-11560-MS, 1989.

[22] P.J. Tennison, T.L. Georjon, P.V. Farrell, R.D. Reitz, An Experimental and Numerical Study of Sprays from a Common Rail Injection System for Use in an HSDI Diesel Engine, in, SAE International, 1998.

[23] L.E. Kollár, M. Farzaneh, A.R. Karev, Modeling droplet collision and coalescence in an icing wind tunnel and the influence of these processes on droplet size distribution, International Journal of Multiphase Flow, 31(1) (2005) 69-92.

[24] T.L. Georjon, R.D. Reitz, A drop-shattering collision model for multidimensional spray computations, Atomization and Sprays, 9(3) (1999).

[25] G. Brenn, D. Valkovska, K. Danov, The formation of satellite droplets by unstable binary drop collisions, Physics of Fluids, 13(9) (2001) 2463-2477.

[26] A. Munnannur, R.D. Reitz, A new predictive model for fragmenting and non-fragmenting binary droplet collisions, International journal of multiphase flow, 33(8) (2007) 873-896.

[27] A. Munnannur, Droplet Collision Modeling in Multi-dimensional Engine Spray Computation, ProQuest, 2007.

[28] A. Munnannur, R.D. Reitz, Comprehensive collision model for multidimensional engine spray computations, Atomization and Sprays, 19(7) (2009).

[29] S. Kim, D.J. Lee, C.S. Lee, Modeling of binary droplet collisions for application to inter-impingement sprays, International Journal of Multiphase Flow, 35(6) (2009) 533-549.

[30] M. Flint, J.-P. Pirault, Opposed piston engines: evolution, use, and future applications, SAE International, Warrendale, PA ISBN, (2009) 978-970.

[31] P. Hofbauer, Opposed Piston Opposed Cylinder (opoc) Engine for Military Ground Vehicles, in, SAE International, 2005.

[32] M. Franke, H. Huang, J.P. Liu, A. Geistert, P. Adomeit, Opposed Piston Opposed Cylinder (opoc™) 450 hp Engine: Performance Development by CAE Simulations and Testing, in, SAE International, 2006.

[33] G. Regner, D. Johnson, J. Koszewnik, E. Dion, F. Redon, L. Fromm, Modernizing the Opposed Piston, Two Stroke Engine for Clean, Efficient Transportation, in, The Automotive Research Association of India, 2013.

[34] S. Naik, D. Johnson, J. Koszewnik, L. Fromm, F. Redon, G. Regner, K. Fuqua, Practical Applications of Opposed-Piston Engine Technology to Reduce Fuel Consumption and Emissions, in, SAE International, 2013.

[35] S.H. Lee, G.H. Ko, H.S. Ryou, A numerical study on the spray-to-spray impingement system, KSME international journal, 16(2) (2002) 235-245.

[36] G.H. Ko, H.S. Ryou, Droplet collision processes in an inter-spray impingement system, Journal of aerosol science, 36(11) (2005) 1300-1321.

[37] T. Chiba, M. Saito, K. Amagai, M. Arai, Inter-spray impingement of two diesel sprays, in: Proc. Int. Conf. Liquid Atomization and Spray Systems (ICLASS), 2000, pp. 16-20.

[38] Y. Maruyama, M. Saito, Effect of Inter-Impingement Process on the Behavior of a Diesel Spray, In: Proc. ILASS-Asia, 2001 (2001) 241-246.

[39] K. Willis, M. Orme, Binary droplet collisions in a vacuum environment: an experimental investigation of the role of viscosity, Experiments in fluids, 34(1) (2003) 28-41.

[40] P.M. Dupuy, Y. Lin, M. Fernandino, H.A. Jakobsen, H.F. Svendsen, Modelling of high pressure binary droplet collisions, Computers & Mathematics with Applications, 61(12) (2011) 3564-3576.

[41] P.J. O'Rourke, A.A. Amsden, The TAB method for numerical calculation of spray droplet breakup, Los Alamos National Lab., NM (USA), 1987.

[42] B.E. Launder, D.B. Spalding, Lectures in mathematical models of turbulence, (1972).

[43] O'Rourke, P. J., Collective drop effects on vaporizing liquid sprays, PhD thesis, Princeton University, New Jersey, 1981.

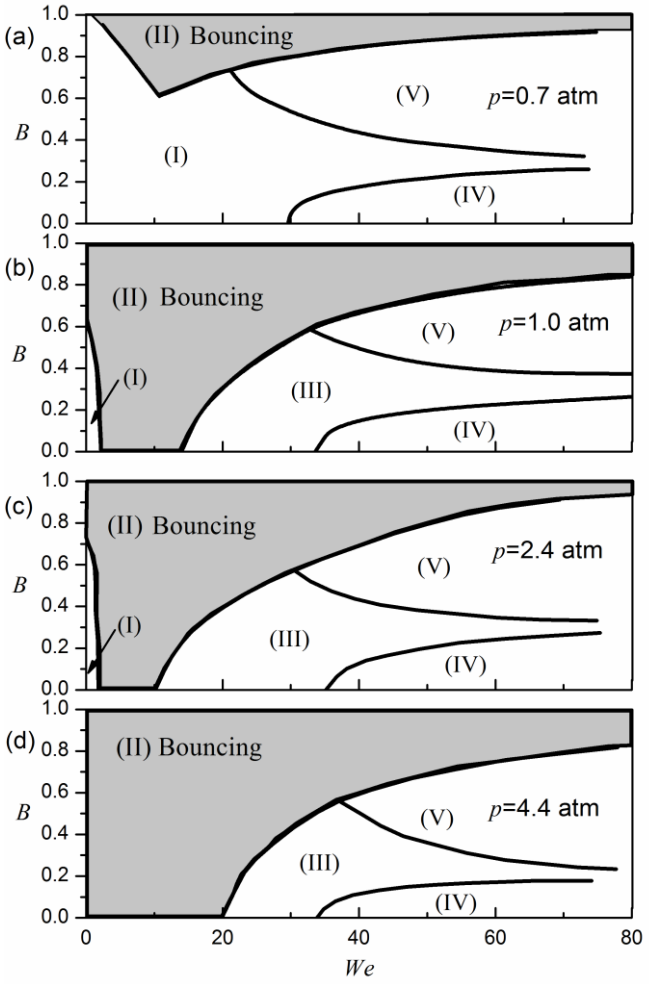

Figure 1. Regime nomograms of n-tetradecane droplet collision at various pressures, adapted from Ref. [8]: (I) coalescence after minor deformation, (II) bouncing, (III) coalescence after substantial deformation, (IV) coalescence followed by separation for near head-on collision (a.k.a. reflective separation), and (V) coalescence followed by separation for off-center collision (a.k.a. stretching separation).

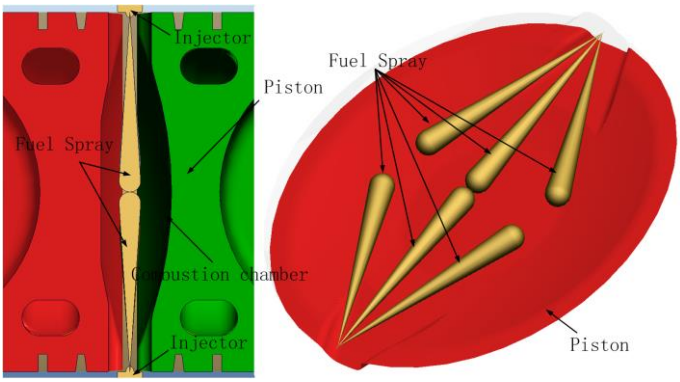

Figure 2. Schematic of fuel injection and multiple impinging sprays in OPCI.

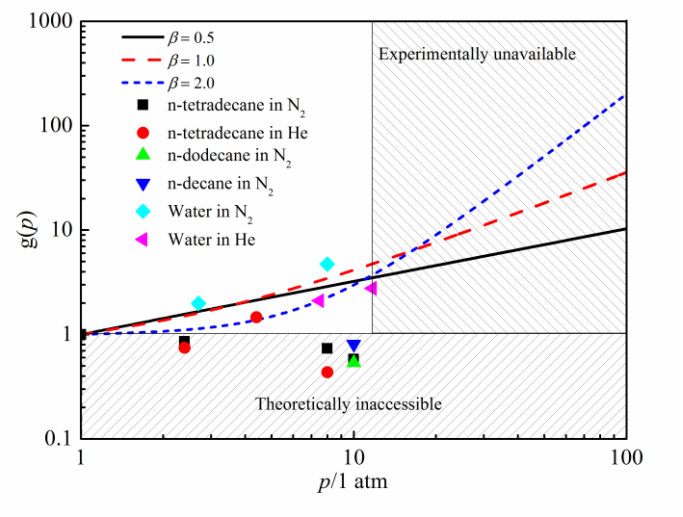

Figure 3. Pressure-dependent factor g(p) by different power-law fittings of $g(p) = ap^{\beta} + b$. The scattered points are adapted from Ref. [8]; the solid line ($\beta = 0.5$) is g(p)=1.03$p^{0.5}$-0.03 with the coefficient of determination R^2=0.584; the dash line ($\beta = 1.0$) is g(p)=0.25p+0.75 with R^2=0.529; and the dotted line($\beta = 2.0$) g(p)=0.02p^2+0.98 with R^2=0.342.

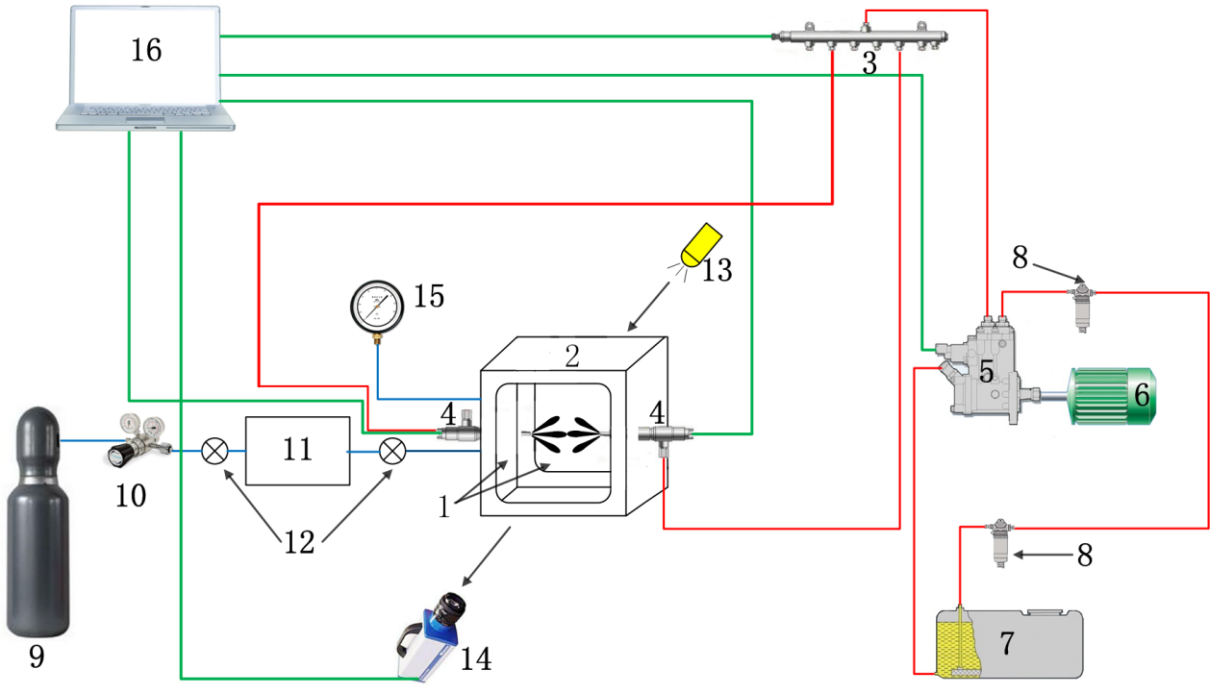

Figure 4. Schematic of experiment apparatus for multiple impinging sprays. (1) Square window, (2) Chamber, (3) Common rail, (4) Injector, (5) Oil pump, (6) Electrical motor, (7) Oil tank, (8) Filter, (9) High pressure cylinder, (10) Reducing valve, (11) Regulator tank, (12) Valve, (13) Stroboscope, (14) High speed Camera, (15) Pressure meter, (16) Control system.

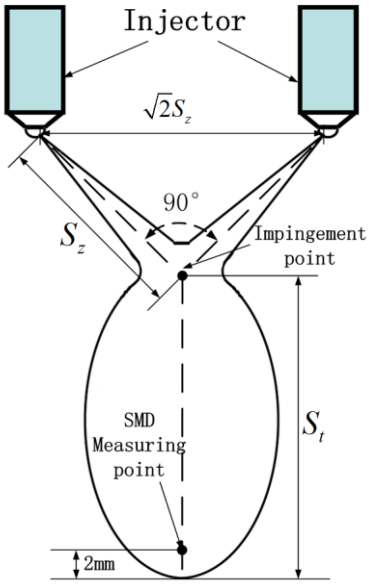

Figure 5. Schematic of the impinging sprays in Maruyama et al.'s experiment [38] at 10 atm.

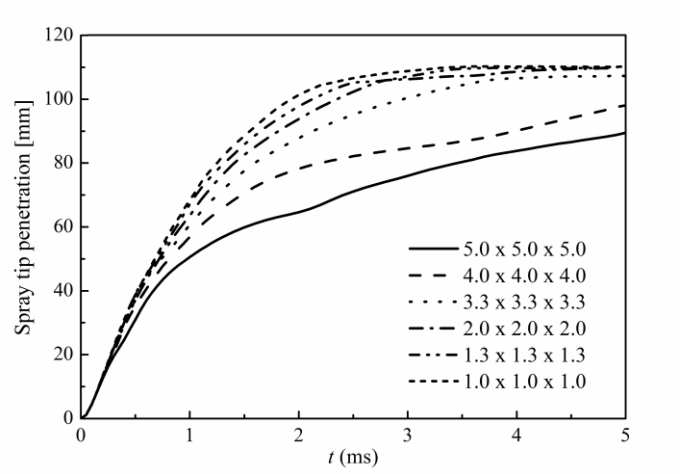

Figure 6. Grid-dependence of the calculated penetration length for the free spray in Maruyama et al.'s experiment [38] at 10 atm.

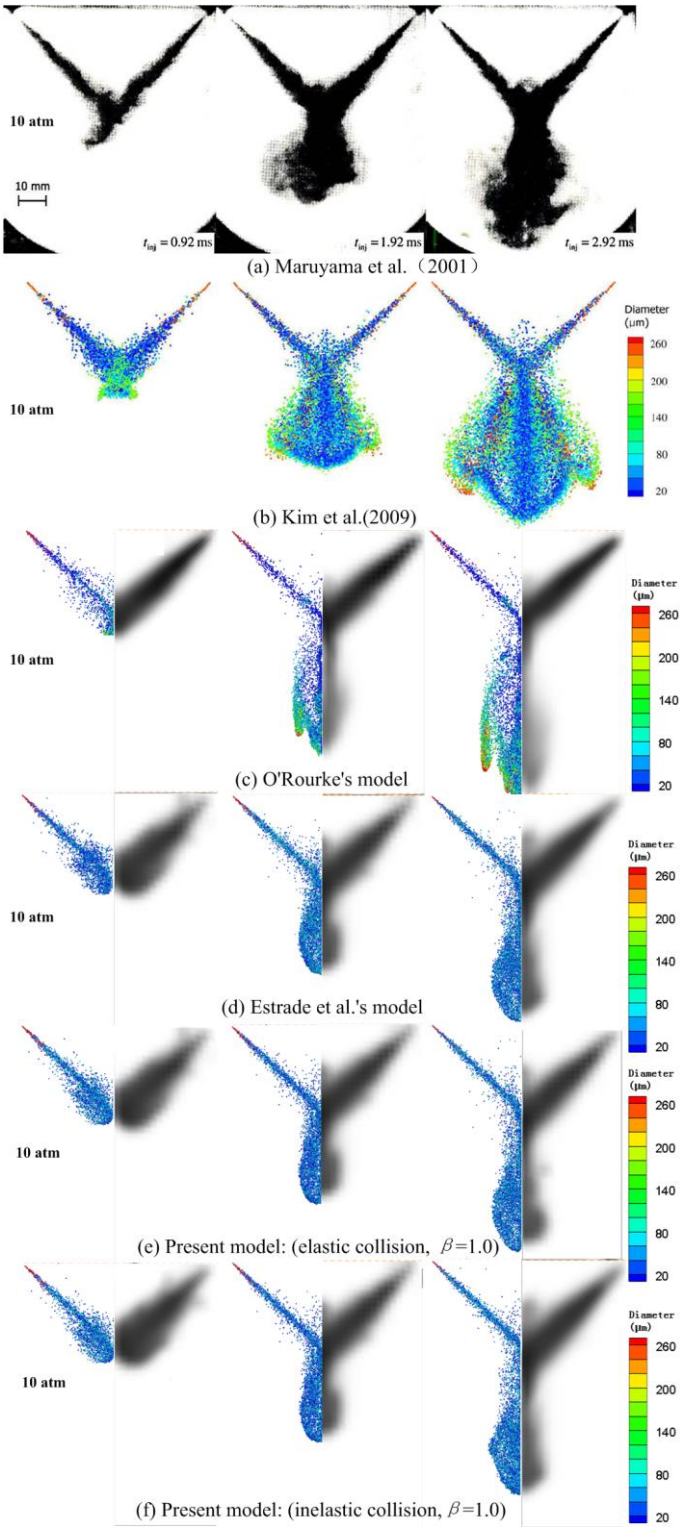

Figure 7. Evolution of impinging sprays with S_z=50mm at 10atm. (a) experimental shadowgraph images (b) Lagrangian droplet parcels predicted in Kim et al.'s [29] simulation, and the present simulation with (c) O'Rourke's model, (d) Estrade et al.'s model, (e) the present model (elastic collision, β=1.0) and (f) the present model (inelastic collision, β=1.0). In graphs (c)-(f), the Lagrangian droplet parcels are shown in the left half and the numerical shadowgraph shown in the right half.

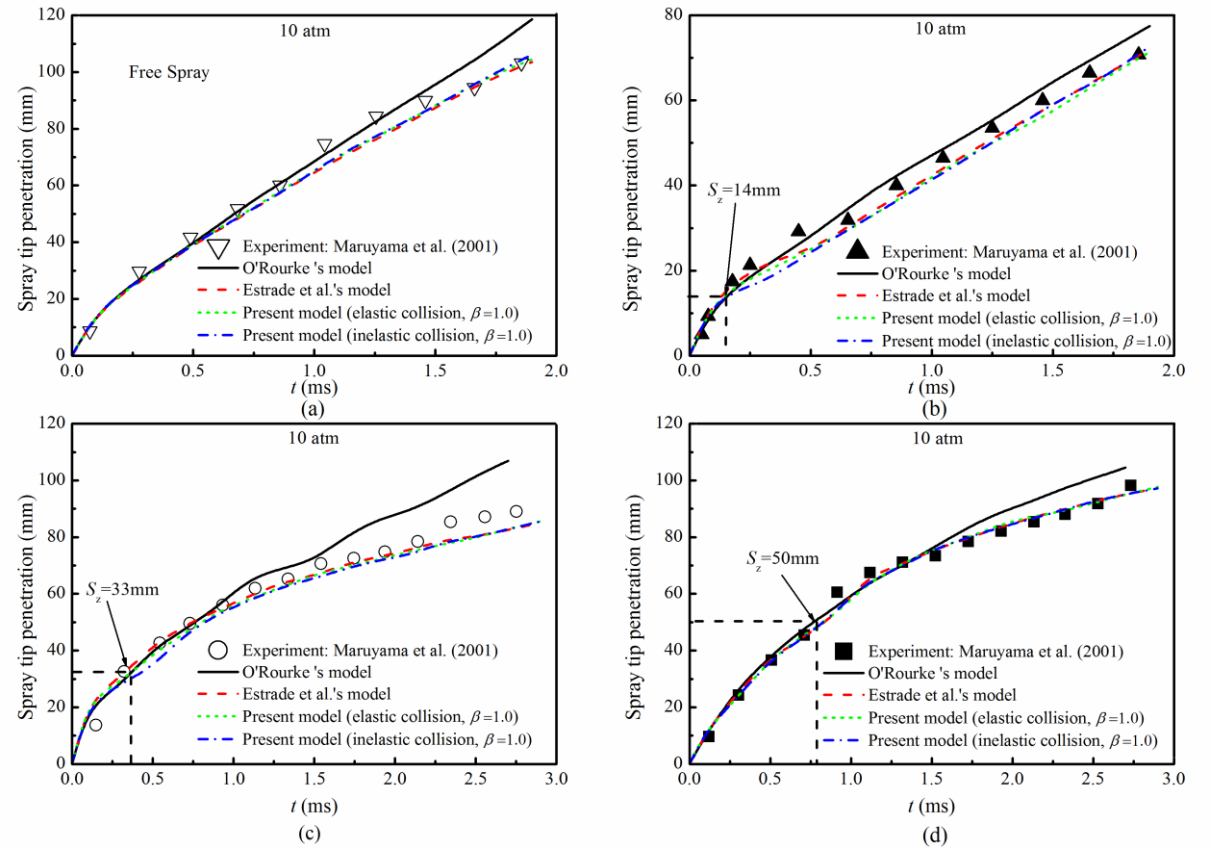

Figure 8. The spray penetration length for (a) free spray, and the impinging sprays with (b) S_z = 14mm, (c) S_z=33 mm and (d) S_z=50 mm at 10 atm. The impingement point and time are indicated in (b)-(d).

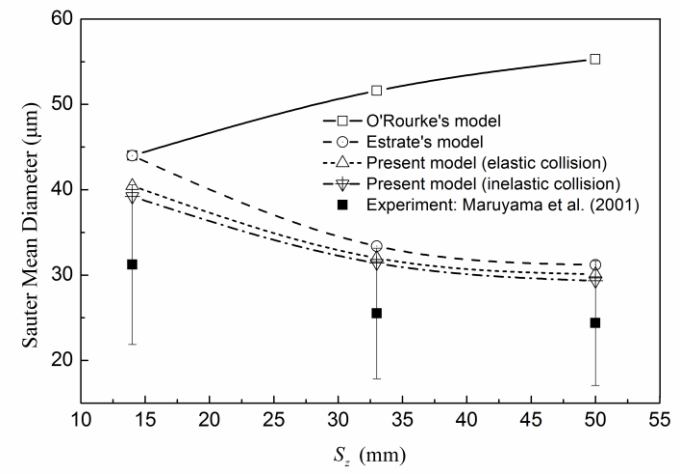

Figure 9. Sauter mean diameter (SMD) at 2 mm above the spray tip and at *t*=2ms for the three impinging sprays of Maruyama et al. [38].

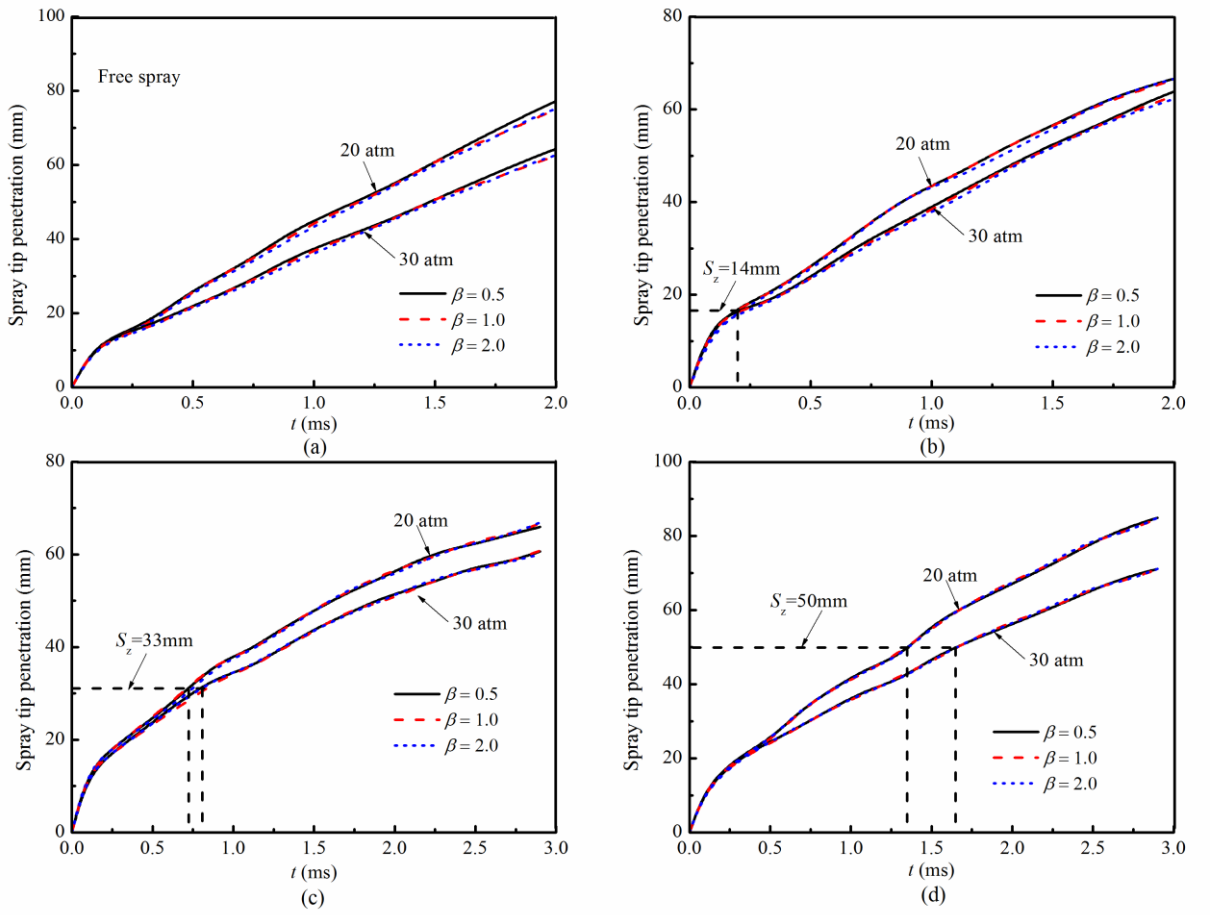

Figure 10. With different power-law fittings and at 20atm and 30atm, the simulated spray penetration length for (a) free spray and the impinging sprays with (b) S_z=14mm, (c) S_z=33mm and (d) S_z=50mm.

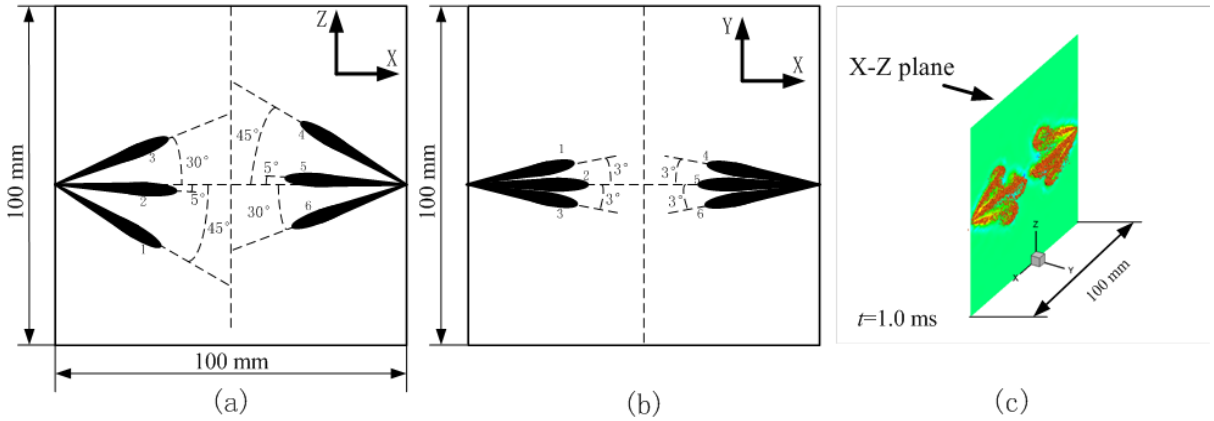

Figure 11. Schematic of the multiple impinging sprays from (a) the front view, (b) the top view and (c) the three-dimensional KIVA-3V simulation at *t*=1.0ms.

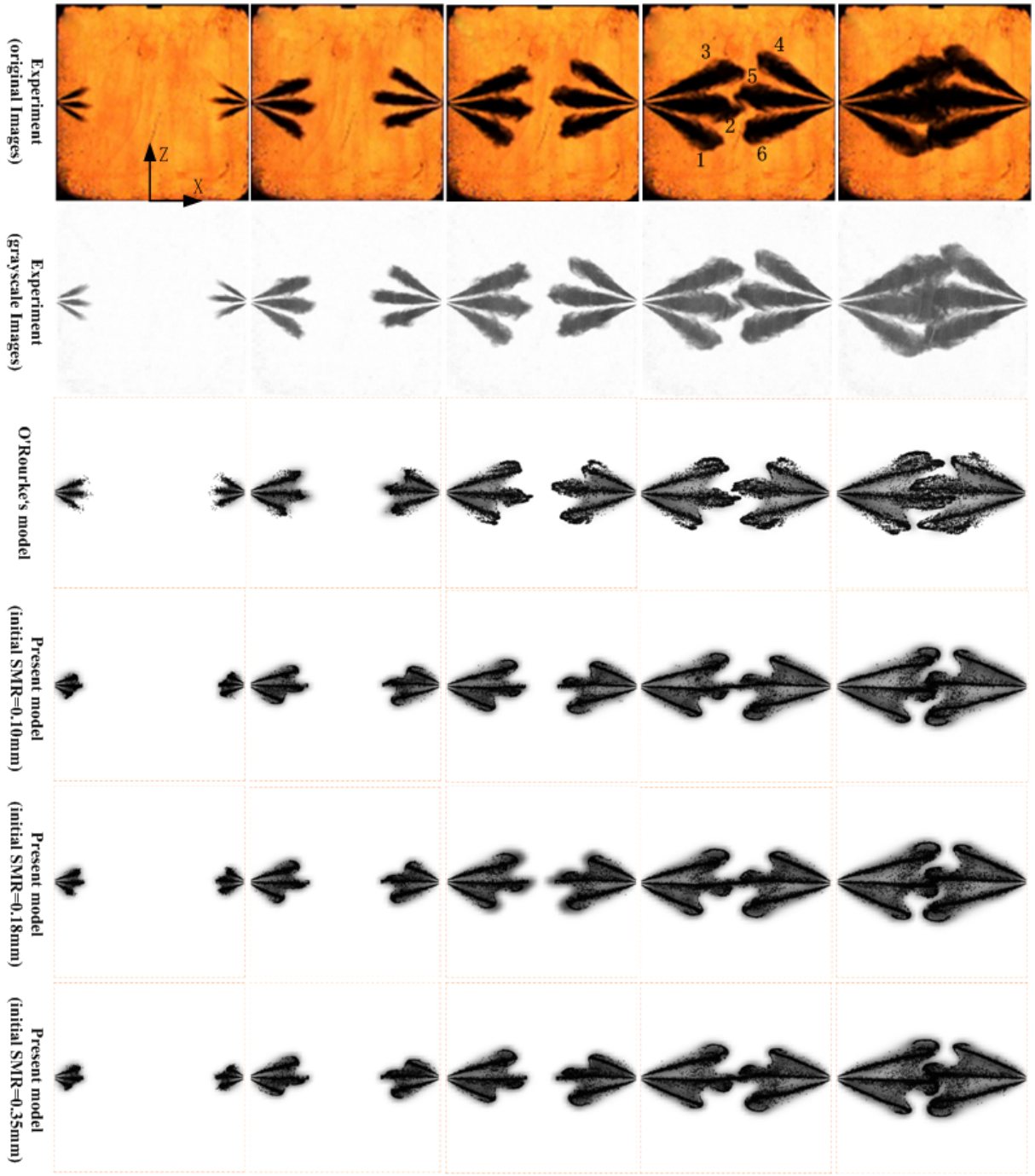
Experiment (original Images)
Experiment (grayscale Images)
O'Rourke's model
Present model (initial SMR=0.10mm)
Present model (initial SMR=0.18mm)
Present model (initial SMR=0.35mm)
Z
X
1
2
3
4
5
6
0.2 ms
0.5 ms
0.8 ms
1.1 ms
1.4 ms

(a)

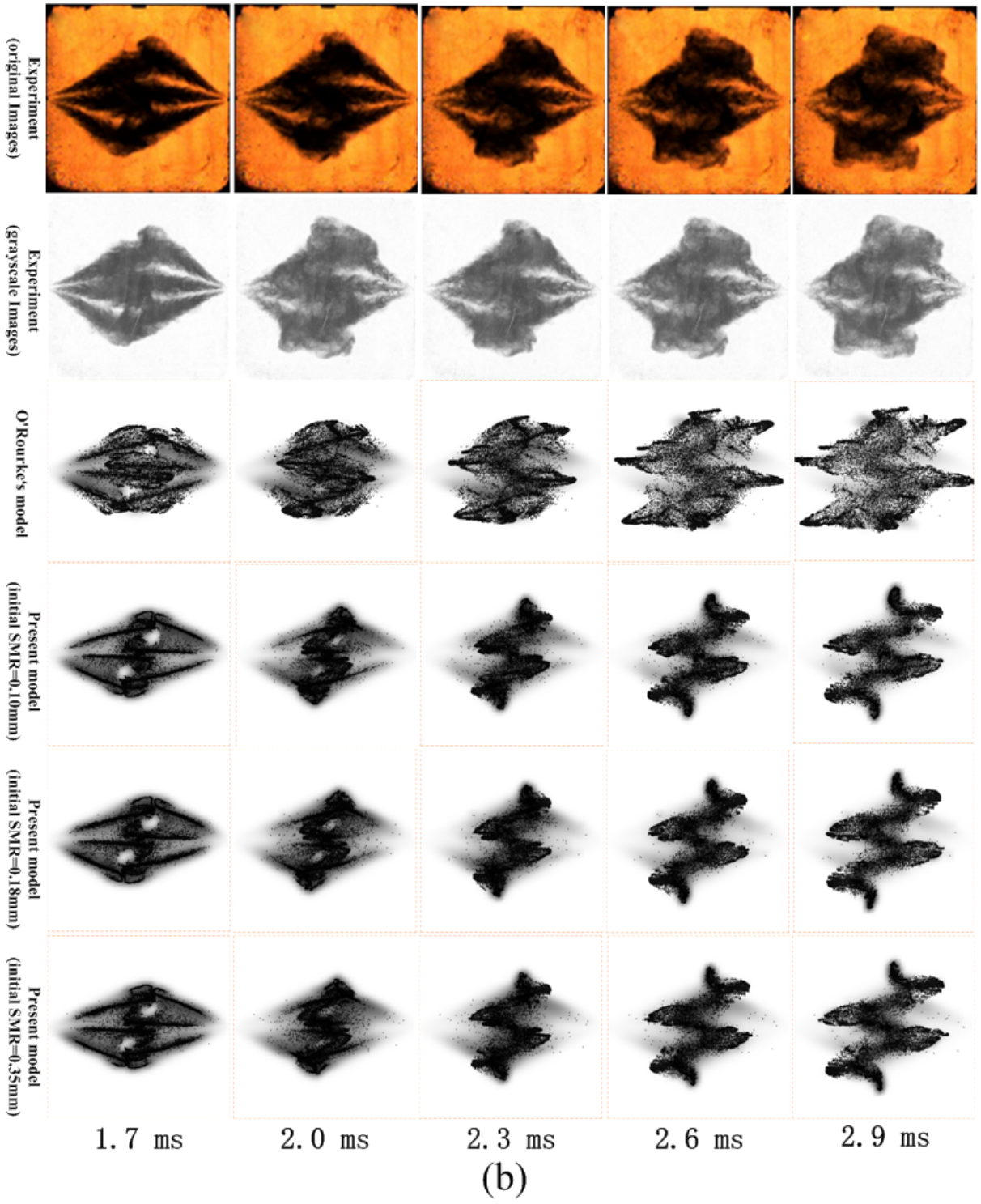

Figure 12. Experimental and numerical shadowgraphs of the multiple impinging sprays at 30 atm during (a) 0.2-1.4ms and (b) 1.7-2.9 ms. Droplet parcels are also shown in the numerical shadowgraphs.

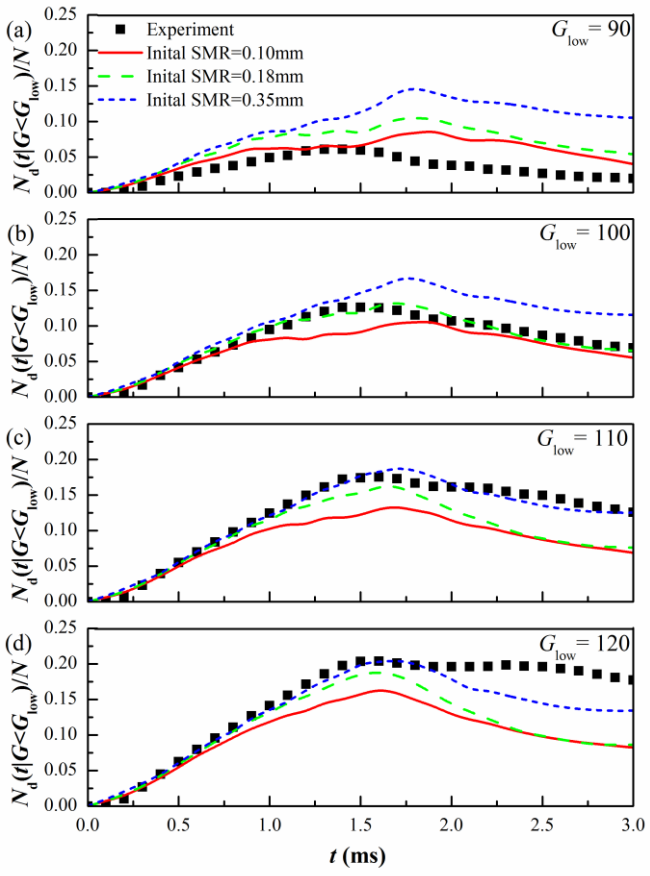

Figure 13. Grayscale level analysis of experimental and numerical shadowgraphs at 30 atm for different initial SMR and for (a) G_{low} = 90, (b) G_{low} = 100, (c) G_{low} = 110 and (d) G_{low} = 120. The numerical shadowgraphs are calculated with the linear fitting.

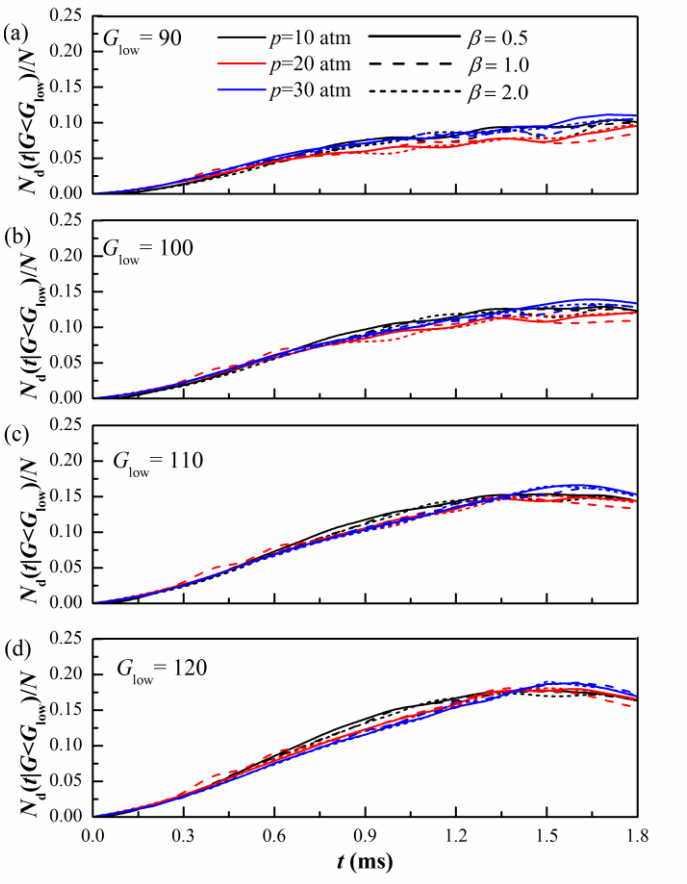

Figure 14. Grayscale level analysis of numerical shadowgraphs with different power-law fittings and at various ambient pressures for (a) G_{low} = 90, (b) G_{low} = 100, (c) G_{low} = 110 and (d) G_{low} = 120.